ACS APPLIED MATERIALS & INTERFACES

Research Article

www.acsami.org

Photoelectrochemical Biosensor Using Enzyme-Catalyzed in Situ Propagation of CdS Quantum Dots on Graphene Oxide

Xianxiang Zeng, Wenwen Tu, Jing Li, Jianchun Bao, and Zhihui Dai*

Jiangsu Collaborative Innovation Center of Biomedical Functional Materials and Jiangsu Key Laboratory of Biofunctional Materials, College of Chemistry and Materials Science, Nanjing Normal University, Nanjing, 210023 Jiangsu, People's Republic of China

ABSTRACT: An innovative photoelectrochemical (PEC) biosensor platform was designed based on the in situ generation of CdS quantum dots (QDs) on graphene oxide (GO) using an enzymatic reaction. Horseradish peroxidase catalyzed the reduction of sodium thiosulfate with hydrogen peroxide to generate H_2S, which reacted with Cd^{2+} to form CdS QDs. CdS QDs could be photoexcited to generate an elevated photocurrent as a readout signal. This strategy offered a "green" alternative to inconvenient presynthesis procedures for the fabrication of semiconducting nanoparticles. The nanomaterials and assembly procedures were characterized by microscopy and spectroscopy techniques. Combined with immune recognition and on the basis of the PEC activity of CdS QDs on GO, the strategy was successfully applied to a PEC assay to detect carcinoembryonic antigen and displayed a wide linear range from 2.5 ng mL^{-1} to 50 μg mL^{-1} and a detection limit of 0.72 ng mL^{-1} at a signal-to-noise ratio of 3. The PEC biosensor showed satisfactory performance for clinical sample detection and was convenient for determining high concentrations of solute without dilution. This effort offers a new opportunity for the development of numerous rapid and convenient analytical techniques using the PEC method that may be applied in the design and preparation of various solar-energy-driven applications.

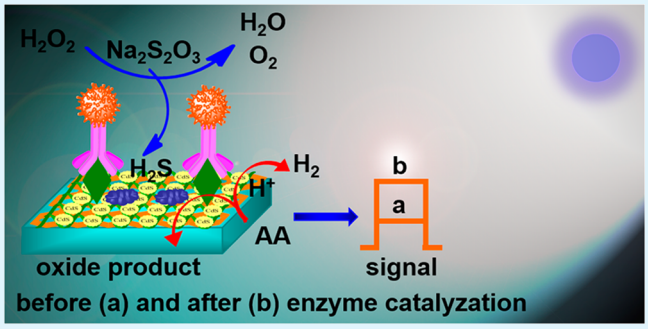

KEYWORDS: *quantum dots, graphene oxide, photoelectrochemistry, enzyme catalysis, biosensing*

INTRODUCTION

Photoelectrochemical (PEC) measurement is a newly emerging and dynamically developing technique for probing various biological events with high sensitivity. PEC measurements combine the advantages of optical methods and electrochemical sensing.[1−11] The principle of PEC biosensors is based on the photocatalytic oxidation or reduction of biomolecules to enable photogenerated electron transfer between the analyte and a semiconductor electrode under light irradiation to amplify the PEC response. In previously reported assays, presynthesized semiconductors have been tethered to recognition elements having an affinity for their target analytes,[5] and a series of PEC platforms have been designed for the detection of small molecules,[3,11−14] thrombin,[15] DNA damage,[16] antigens,[17,18] and cells.[7,19]

However, the use of presynthesized semiconductors as a signal source for PEC platforms has several drawbacks, such as harsh operating conditions and time-consuming fabrication processes, which potentially cause high background signals, low sensitivity, and increased cost of analytical assays and is unfavorable for simplifying PEC detection and in situ monitoring of tumor markers. In fluorescence-based analyses, the enzyme-catalyzed growth of quantum dots (QDs) is a promising substitute for the use of a presynthesized semiconductor. Acetylcholine esterase can catalyze the conversion of acetylthiocholine to yield thiocholine, which promotes the decomposition of $S_2O_3^{2-}$ to H_2S;[20,21] the subsequent reaction of H_2S with Cd^{2+} forms CdS QDs, thereby improving the sensitivity of fluorescence analysis.[22,23] Alkaline phosphatase (ALP) catalyzes the hydrolysis of *p*-nitrophenyl phosphate, which generates *p*-nitrophenol and inorganic phosphate. The inorganic phosphate stabilizes the QDs produced in situ through the interaction of Cd^{2+} with S^{2-} ions, which offers a more stable fluorescence signal.[24]

On the basis of these previous studies, we considered that the enzyme-catalyzed growth of QDs could be developed for the detection of various biomolecules. To the best of our knowledge, no reports have focused on the enzyme-catalyzed in situ propagation of QDs for PEC biosensors. This technique differed from the ALP-catalyzed hydrolysis of ascorbic acid 2-phosphate to generate an electron donor to modify presynthesized TiO_2, which was utilized for the detection of an ALP inhibitor.[14] However, this reaction was not applied in our work. In this system, $Na_2S_2O_3$ should be reduced to H_2S in the presence of H_2O_2. Horseradish peroxidase (HRP) is an enzyme which can catalyze the reaction of H_2O_2. Therefore, the rate of the reaction could be significantly improved with the help of HRP. Then the generated H_2S reacted with Cd^{2+} to

Received: July 3, 2014
Accepted: August 25, 2014
Published: August 25, 2014

form CdS QDs, which was called enzyme-catalyzed growth of QDs. By virtue of the immune recognition reaction, HRP was introduced to catalyze the propagation of CdS QDs, which could be photoexcited to generate a photocurrent as a readout signal, thereby generating a detector for tumor markers. Specifically, water-soluble graphene oxide (GO) was adopted to improve the stability of CdS QDs and reduce the recombination of electron−hole pairs to increase the PEC signal. The use of GO was advantageous for many applications, including sensors, optical and electronic devices, and energy conversion and storage.[25−31] Furthermore, GO was cheaper and more environmentally friendly than its derivatives. Meanwhile, GO possessed a band between CdS QDs and the indium tin oxide (ITO) electrode. It might be a good intermedium for electron transfer from the ITO electrode to CdS QDs. In addition, GO could facilitate CdS QD$^{\bullet+}$ production and trigger $O_2^{\bullet-}$ generation[32,33] and was acted as a vehicle for proton (H^+) transport.[27] GO can generate a photocurrent upon light irradiation[34,35] and may be used as the source of the PEC signal.

Here, using carcinoembryonic antigen (CEA) as a model, a novel PEC biosensor protocol based on the in situ generation of CdS QDs for CEA detection was proposed (Scheme 1).

Scheme 1. Schematic Illustration of the Assembly Process of the PEC Biosensor

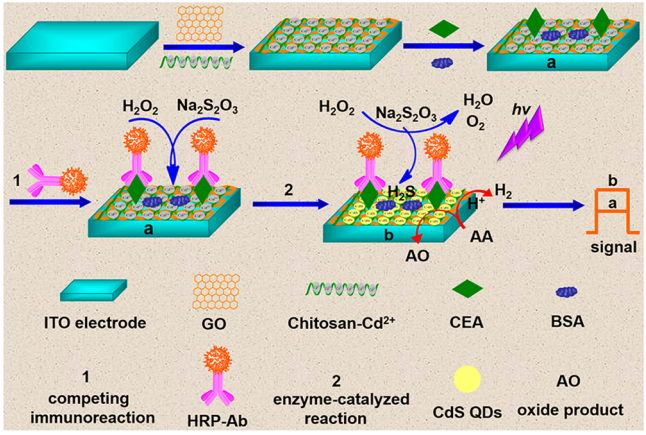

Through a competitive immune recognition reaction, CEA was specifically conjugated to its HRP-labeled anti-CEA antibody (HRP-Ab). HRP then catalyzed the reduction of $Na_2S_2O_3$ with H_2O_2 to generate H_2S and form CdS QDs, which could be photoexcited under visible light to produce a photocurrent as the determination signal. The specific interaction between the CEA and HRP-Ab could be detected by recording the enhanced photocurrent of CdS QDs sensitized by GO.

EXPERIMENTAL SECTION

Materials and Reagents. Graphite (99.95%, 8000 mesh) was obtained from Aladdin Industrial Corp. Chitosan (CS), glutaraldehyde (GLD) solution (50%), and bovine serum albumin (BSA) were obtained from Sigma-Aldrich. Cadmium acetate ($Cd(CH_3COO)_2\cdot 2H_2O$) was purchased from Shanghai Reagent Co., Ltd. (Shanghai, China). CEA and HRP-Ab were purchased from Beijing Keybiotech Co., Ltd. (China). Ascorbic acid (AA) and H_2O_2 (30%) were obtained from Sinopharm Chemical Reagent Co., Ltd. (China). Other chemicals were of analytical reagent grade. The washing solution was tris(hydroxymethyl)aminomethane−hydrochloric acid (Tris−HCl) buffered saline (10 mmol L^{-1}, pH 7.4). The washing solution containing BSA (1%, w/v) was used as the blocking solution. Tris−HCl buffered saline (0.1 mol L^{-1}, pH 7.4) containing 0.1 mol L^{-1} AA was used as the test solution. Ultrapure water obtained from a Millipore water purification system (≥18 MΩ·cm, Millipore, United States) was used in all assays. Blood samples from the Jiangsu Hospital of Cancer were centrifuged at 4000 rpm for 5 min to obtain the supernates as clinical serum samples. CEA solutions (20 μL) with different concentrations were mixed with HRP-Ab (20 μL, 60 μg mL^{-1}) to obtain the incubation solution.

The films deposited on ITO were collected from multiple groups by the blade after the enzyme catalyzation. One part was used for Fourier transform infrared (FTIR) measurements, and the other was processed to form a suspension with slightly ultrasonic treatment in ultrapure water with a short time for ultraviolet−visible (UV−vis) absorption spectral tests and to obtain transmission electron microscopy (TEM) and high-resolution TEM (HRTEM) images. The samples which were obtained from the incubation solution (C_{CEA} = 10 μg mL^{-1}) were prepared for all the characterizations except where otherwise indicated.

Apparatus. The PEC measurements were performed with a Zahner PEC workstation (Zahner, Germany). All experiments were carried out at room temperature using a conventional three-electrode system with a modified ITO electrode (sheet resistance 20−25 Ω/square) with a geometrical area of 1.0 ± 0.1 cm^2 as the working electrode, a platinum wire as the auxiliary electrode, and a Ag/AgCl electrode as the reference electrode. All of the PEC measurements were carried out under 405 nm of irradiation at a constant potential of −0.2 V (versus Ag/AgCl) in Tris−HCl (0.1 mol L^{-1}, pH 7.4) buffered saline containing AA (0.1 mol L^{-1}), which was deaerated with high-purity nitrogen for 15 min before PEC experiments and then kept over a N_2 atmosphere for the entire experimental process. The HRTEM images were obtained on a JEOL-2100F apparatus at an accelerating voltage of 400 kV (JEOL, Japan). Electrochemical impedance spectroscopy (EIS) was carried out at open circuit potential with an Autolab potentiostat/galvanostat PGSTAT302N (Metrohm, The Netherlands) and controlled by Nova 1.8 software with a three-electrode system in KCl solution (0.1 mol L^{-1}) containing a $K_3Fe(CN)_6/K_4Fe(CN)_6$ (5.0 mmol L^{-1}) (1:1) mixture as the redox probe from 0.1 Hz to 100 kHz with a signal amplitude of 10 mV. TEM images were taken using a Hitachi H-7650 type transmission electron microscope at an accelerating voltage of 80 kV (Hitachi, Japan). UV−vis absorption spectra were obtained on a Cary 60 spectrophotometer (Agilent, United States). FTIR spectra were acquired in the range of 4000−400 cm^{-1} on a Tensor 27 (Bruker, Germany) at room temperature.

Synthesis of GO. GO was synthesized using a modified version of the Hummers method.[36] In detail, graphite (2 g) was mixed with concentrated H_2SO_4 (10 mL), $K_2S_2O_8$ (1 g), and P_2O_5 (1 g). The solution was heated to 80 °C and stirred for 6 h in an oil bath. The mixture was then diluted with deionized water, and the product was obtained by filtration through a 0.2 μm Nylon film and dried under ambient conditions. Thereafter, the product was reoxidized by adding $KMnO_4$ (0.6 g) to concentrated H_2SO_4 (10 mL) containing 0.2 g of the preoxidized products. After the resulting solution was stirred for 2 h at 35 °C, deionized water (9.2 mL) was added followed by additional deionized water (28 mL) and H_2O_2 (0.5 mL) with continuous stirring for 15 min. During the above process, a light yellow hydrosol was obtained. The light yellow hydrosol was washed with concentrated hydrochloric acid (10 mL) and deionized water (100 mL). After centrifugation and ultrasonic dispersion, the final product was dried under vacuum. The product was diluted and sonicated for 1 h to separate any aggregated graphite oxide layers and further centrifuged to remove any graphite oxide residue prior to use.

CS (0.5 mg) was added to 1 mL of a 1% acetic acid solution and ultrasonicated for 3 h to obtain a uniform CS solution. Cd-$(CH_3COO)_2\cdot 2H_2O$ (16.0 mg) was then added to obtain a homogeneous solution.

Preparation of the PEC Biosensor. A GO solution (25 μL, 1 mg mL^{-1}) was coated onto the ITO electrode (ITO/GO). Before drying, a CS (0.05%, 20 μL) solution containing $Cd(CH_3COO)_2\cdot 2H_2O$ (0.06 mmol L^{-1}) was dropped onto the electrode surface. After GLD (1%,

20 μL) was reacted with CS for 30 min, CEA (60 μg mL^{-1}, 20 μL) was conjugated onto the electrode and placed at 4 °C overnight to obtain ITO/GO/CEA. To eliminate nonspecific adsorption, any possible remaining active sites were blocked by placing the electrode in blocking solution (20 μL) for 1 h. After the electrode was rinsed with washing solution, the PEC biosensor (ITO/GO/CEA/BSA) was obtained. Thorough washing with wash solution was required at each assembly step.

PEC Tests. The incubation solution (20 μL) was dropped onto the PEC biosensor and incubated for 45 min to obtain ITO/GO/CEA/BSA/HRP-Ab. Then $Na_2S_2O_3$ (1.8 mmol L^{-1}, 20 μL) and H_2O_2 (2.6 mmol L^{-1}, 20 μL) were cast onto the electrode and reacted for 15 min to obtain ITO/GO/CEA/BSA/HRP-Ab/CdS. Finally, after thorough washing, ITO/GO/CEA/BSA/HRP-Ab/CdS was inserted into the test solution to record the PEC response at an applied potential of −0.2 V with 405 nm irradiation under a N_2 atmosphere.

RESULTS AND DISCUSSION

Characterization of GO, GO−CdS Nanocomposites, and the PEC Biosensor. GO was characterized using the UV−vis absorption spectrum and TEM (Figure 1). The UV−vis absorption spectrum of GO exhibited two characteristic adsorption peaks: a peak at 230 nm due to the $\pi \rightarrow \pi^*$ transition of the C═C bond and a shoulder at approximately 300 nm corresponding to the $n \rightarrow \pi^*$ transition of the C═O bond (Figure 1A).[37,38] Meanwhile, Figure 1B shows the representative TEM image of GO. The veil-like GO sheets exhibited a wrinkle on the surface, which supplied a superior three-dimensional structure for CdS QD deposition.

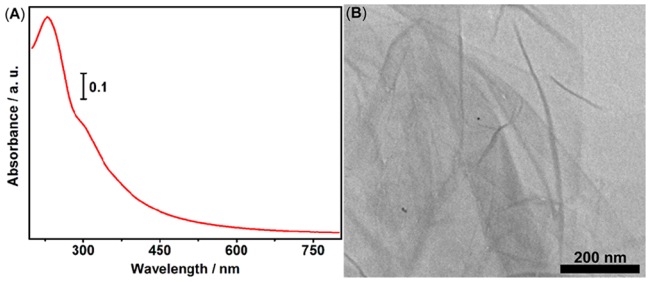

Figure 1. (A) UV−vis absorption spectrum and (B) TEM image of GO.

The UV−vis absorption spectra were used to characterize the formation of CdS QDs on GO (Figure 2A). Compared with the spectrum of GO (curve a), a broad peak (approximately 400 nm) appeared after modification of HRP-Ab (curve c), which was verified by the pure HRP (60 μg mL^{-1}) absorption spectrum (curve b).[8] When HRP catalyzed the reduction of $Na_2S_2O_3$ by H_2O_2 to generate H_2S, which reacted with Cd^{2+} on GO,[23] the absorption intensified (curve d), indicating the formation of CdS QDs. The possible reaction equations at the sensor surface were as follows:[20,32,33]

$$6H_2O_2 + 2S_2O_3^{2-} \xrightarrow{HRP} 4OH^- + 4H_2S + 7O_2 \quad (1)$$

$$4OH^- + 2H_2S \rightarrow 2H_2O + S^{2-} \quad (2)$$

$$S^{2-} + Cd^{2+} \rightarrow CdS \quad (3)$$

$$H_2S + Cd^{2+} \rightarrow 2H^+ + CdS \quad (4)$$

$$OH^- + H^+ \rightarrow H_2O \quad (5)$$

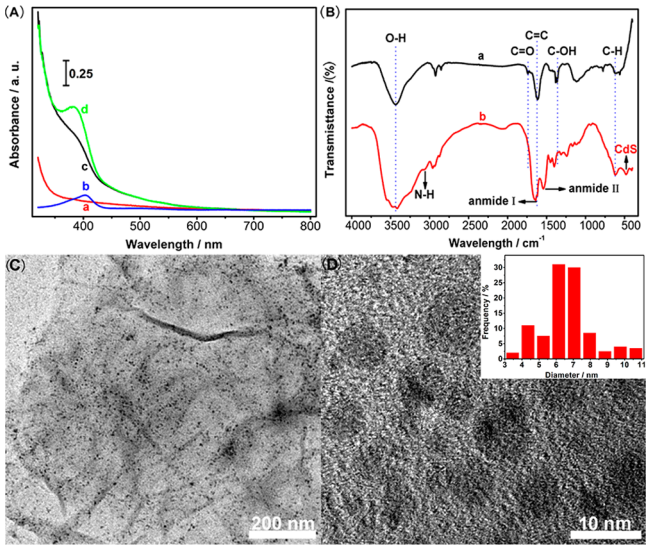

Figure 2. (A) UV−vis absorption spectra of GO, HRP, GO/CEA/BSA/HRP-Ab, and GO/CEA/BSA/HRP-Ab/CdS (a−d). (B) FTIR spectra of (a) GO and (b) GO/CEA/BSA/HRP-Ab/CdS. (C) TEM and (D) HRTEM images of GO/CEA/BSA/HRP-Ab/CdS. Inset in (D): size distribution of CdS QDs.

$$CdS + In{-}SnO_x \xrightarrow{GO} CdS^{\bullet+} + In{-}SnO_x^{\bullet-} \quad (6)$$

$$O_2 + In{-}SnO_x^{\bullet-} \xrightarrow{GO} O_2^{\bullet-} + In{-}SnO_x^{-} \quad (7)$$

$$CdS^{\bullet+} + O_2^{\bullet-} \xrightarrow{GO} CdS^* + O_2 \quad (8)$$

$$CdS^* + AA \rightarrow AO + CdS \quad (9)$$

FTIR spectroscopy further confirmed the generation of CdS on GO (Figure 2B). Compared with the major peaks of GO in the FTIR spectrum (curve a), in addition to the C═O (1740 cm^{-1}), C═C (1618 cm^{-1}), and O−H (3415 cm^{-1}) vibrations, the FTIR signal of GO/CEA/BSA/HRP-Ab/CdS showed other vibrations corresponding to amide A (3070 cm^{-1}, mainly N−H stretching vibrations), amide I (1639 cm^{-1}, mainly C−O stretching vibrations), amide II (1541 cm^{-1}, the coupling of bending vibrations of N−H and stretching vibrations of C−N), and Cd−S (486 cm^{-1}) (curve b).[39] Furthermore, TEM (Figure 2C) and HRTEM (Figure 2D) images provided direct evidence for the formation of CdS QDs. The HRTEM image clearly showed well-defined individual CdS QDs (Figure 2D), which confirmed the formation of CdS QDs by HRP catalysis. Moreover, the average size of individual CdS QDs was estimated to be 6.6 nm (Figure 2D, inset). The oxygen-containing groups on GO, which are negatively charged, could supply fine propagation sites for Cd^{2+} [31] and lead to the narrow size distribution of CdS QDs, which is beneficial for fabricating the PEC biosensor. After the CS was deposited, it had three effects: as an entrapping agent for GO, in cross-linking reaction with GLD, and as a coordinating reagent with Cd^{2+} because of its rich oxygen groups. GO and CS stabilized the Cd^{2+} on the electrode readily reacting with H_2S to form CdS QDs. After the groups of CS and GLD were activated via the cross-linking reaction, the CEA and BSA could easily be assembled on the electrode, and the PEC biosensor (ITO/GO/CEA/BSA) was prepared after washing.

A photocurrent was generated (Figure 3A, curve a) after 20 μL of GO solution (Figure 4A) was cast onto the ITO

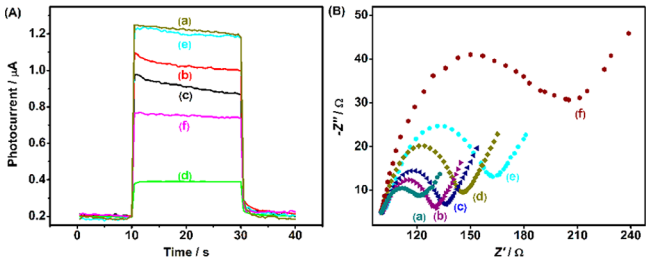

Figure 3. (A) PEC responses of ITO/GO, ITO/GO/CEA, ITO/GO/CEA/BSA, ITO/GO/CEA/BSA/HRP-Ab, ITO/GO/CEA/BSA/HRP-Ab (0 μg mL^{-1} CEA)/CdS, and ITO/GO/CEA/BSA/HRP-Ab (10 μg mL^{-1} CEA)/CdS (a–f). (B) EIS spectra of ITO, ITO/GO, ITO/GO/CEA, ITO/GO/CEA/BSA, ITO/GO/CEA/BSA/HRP-Ab, and ITO/GO/CEA/BSA/HRP-Ab/CdS (a–f).

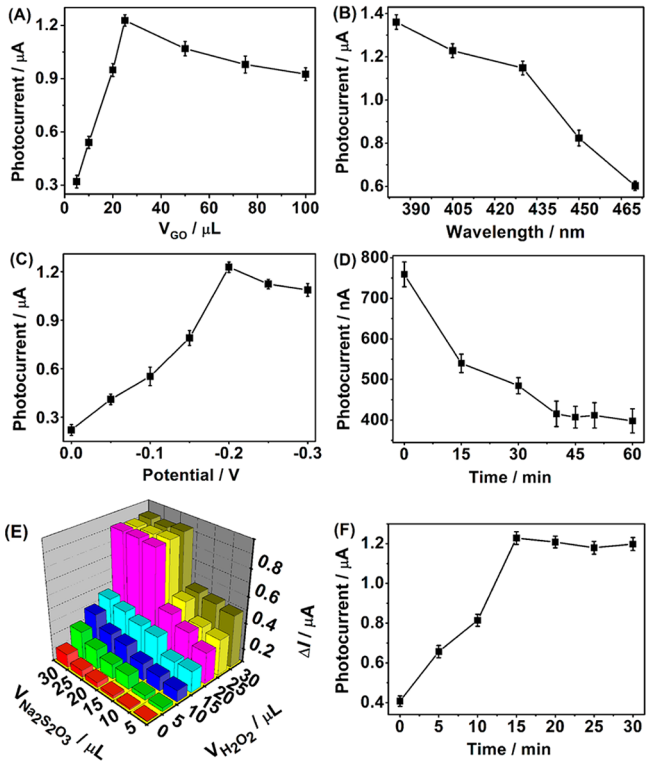

Figure 4. Effects of (A) GO content, (B) excitation wavelength, (C) applied potential, (D) incubation time, (E) $Na_2S_2O_3$ and H_2O_2 content, and (F) reaction time on the PEC response obtained in the test solution.

electrode, which was irradiated by 405 nm light at an applied potential of −0.2 V (Figure 4B,C).[28,40,41] As the steric hindrance of the protein layer impeded AA diffusion onto the electrode surface to scavenge holes and block photogenerated electron transfer, the photocurrent decreased successively with the assembly of CEA, BSA, and HRP-Ab (C_{CEA} = 0 μg mL^{-1}) (Figure 3A, curves b–d) after a 45 min incubation (Figure 4D). In the presence of $Na_2S_2O_3$ (25 μL) and H_2O_2 (25 μL) (Figure 4E), an enhanced photocurrent was obtained (Figure 3A, curve e) after the HRP-catalyzed reaction proceeded for 15 min (Figure 4F). This was attributed to the formation of photoactive CdS QDs, which sensitized GO and led to an improved PEC response. At a negatively applied bias, the holes generated in the valence band of CdS QDs were scavenged by AA. Simultaneously, along with H^+ in Tris–HCl buffered saline, AA was served as a H^+ source for H_2 production in the conduction band of CdS QDs at the GO surface.[34,35] With interaction with the incubation solution (C_{CEA} = 10 μg mL^{-1}) (Figure 3A, curve f), the photocurrent was higher than that of curve d but lower than that of curve e, which might have occurred because less HRP-Ab could conjugate with CEA immobilized on the electrode, which resulted in a decreased number of CdS QDs formed by HRP catalysis.

EIS was an effective method for monitoring changes in the assembly process (Figure 3B). Due to its nonconductive properties, GO could inhibit electron transfer and lead to increased electron transfer resistance (R_{et}) for the redox probe (curve b) compared with a bare ITO electrode (curve a). Proteins with insulative properties would obstruct the diffusion of the redox probe to the electrode and increase the resistance. This premise was consistent with the observed increased R_{et} value after the anchoring of CEA, BSA, and HRP-Ab (curves c–e). After the HRP catalysis reaction, the R_{et} value was greatly increased (curve f). This phenomenon was ascribed to CdS QD propagation that further impeded the redox probe transfer, which is in agreement with the results of the spectra and microscopy images shown in Figure 2.

Optimization of the Detection Conditions. The detection conditions were optimized for PEC determination. The photocurrent increased as the volume of GO (V_{GO}) was increased from 5 to 25 μL (Figure 4A). A maximum photocurrent was observed at 25 μL and then decreased with additional GO, which might have been due to the excessive deposition of GO on the electrode and inhibition of electron and proton transport. Therefore, 25 μL was selected as the optimal deposition volume.

The irradiation wavelength was an important factor that influenced the PEC response. As observed at an applied potential of −0.2 V, the photocurrent decreased and excitation wavelength increased from 385 to 470 nm (Figure 4B). The photocurrents at 405, 430, and 450 nm were 90.3%, 84.4%, and 60.5%, respectively, of that at 385 nm. The photocurrent at 405 nm provided sufficient sensitivity for PEC detection. Moreover, the absorption band of CdS QDs was approximately 400 nm (Figure 2A, curve d); however, 405 nm was more suitable for the excitation of CdS QDs. Therefore, 405 nm was chosen for PEC determination.

The applied potential was also an important parameter for producing the photocurrent. As shown in Figure 4C, the photocurrents increased from 0 to −0.2 V when the irradiation wavelength was 405 nm and reached its maximum. Thereafter, the photocurrent decreased as the applied potential was increased from −0.2 to −0.3 V, which might be attributed to the reduction of oxygen-containing groups at negative potentials less than −0.2 V.[38] The decreased bias potential could inhibit proton adsorption for electron consumption and electron–hole pair separation, which would reduce the photocurrent. Because of the addition of light energy consumption, the excited electron can be driven more easily from the conduction band to the electrolyte under lower potential and vice versa. Therefore, photoelectrochemical biosensing needs a lower oxidation potential than electrochemical and chemiluminescence methods. Moreover, the low applied potential was beneficial for the elimination of interference from other species in the samples. Therefore, −0.2 V was selected for PEC detection.

The effect of the incubation time on the response of the PEC biosensor is presented in Figure 4D. The photocurrent leveled off after 45 min, which was indicative of the immune reaction

having reached equilibrium. Consequently, 45 min was selected as the incubation time for the PEC biosensor.

Furthermore, the contents of $Na_2S_2O_3$ and H_2O_2 were assessed to obtain an optimal PEC response for the system (Figure 4E). The photocurrent increased with increasing volume of H_2O_2 and displayed slight variation with increasing volume of $Na_2S_2O_3$. The increased photocurrent may be due to H_2O_2 as opposed to $Na_2S_2O_3$, which could be acted as an electron and proton donor for the photocurrent generation in the system. The PEC response achieved a plateau in the presence of H_2O_2 (25 μL) and $Na_2S_2O_3$ (25 μL) and fluctuated slightly thereafter. Accordingly, a H_2O_2 and $Na_2S_2O_3$ volume of 25 μL was selected for the enzyme-catalyzed reaction.

The optimal duration of the enzyme-catalyzed reaction was also determined (Figure 4F). The photocurrent leveled off after 15 min, indicating that the reaction attained its maximum. Thus, 15 min was chosen as the optimal enzyme catalysis reaction time.

PEC Biosensing. The PEC biosensing concept was developed to provide a quantitative means to analyze the target. CEA was selected as a model of clinical heterogeneous immunoassays in human serum and was detected under optimal conditions (Figure 4) by this PEC biosensor. Prior to the assay, the ITO/GO/CEA/BSA electrode was directly inserted into the incubation solution without CEA as a control experiment. No obvious difference in the photocurrent was observed compared to the background signal, suggesting that nonspecific binding was attenuated. The photocurrents were measured by varying the CEA concentrations in the incubation solution, and the results are presented in Figure 5A. When the

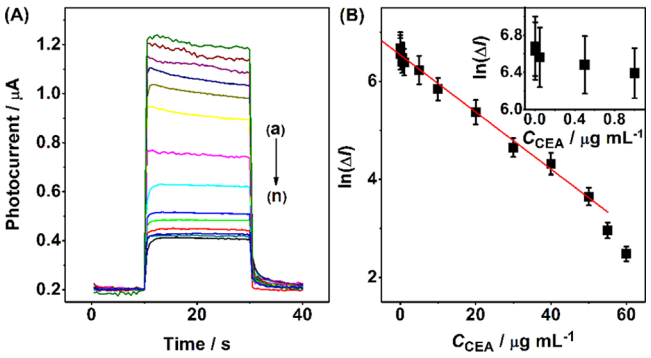

Figure 5. (A) PEC responses and (B) corresponding calibration curve of the biosensor to (a–n) 0, 0.0025, 0.005, 0.05, 0.5, 1, 5, 10, 20, 30, 40, 50, 55, and 60 μg mL^{-1} CEA. Inset: linear range from 0.0025 to 1 μg mL^{-1} for CEA.

concentration of CEA was increased, the corresponding photocurrent decreased and inversely correlated with the concentration of CEA. A calibration plot for the photocurrent (ln ΔI) was obtained by plotting the difference between the photocurrent at different CEA concentrations (C) and the background reading as a function of C; this plot of corrected photocurrent versus C showed a linear response from 2.5 ng mL^{-1} to 50 μg mL^{-1} (Figure 5B). The detection limit was 0.72 ng mL^{-1} at a signal-to-noise ratio of 3.

The linear response range was much broader than the 1.0–60 ng mL^{-1} range achieved by the chemiluminescence method[39] as well as the 20–2000 ng mL^{-1} range determined by surface plasmon resonance imaging.[42] In addition, the detection potential (−0.2 V) was more similar to the physiological potential than −0.84 V, which was determined by the electrochemical method,[43] and 0.64 V, which was determined by the electrochemiluminescence (ECL) method,[44] thereby leading to less interference. Notably, the upper detection limit (50 μg mL^{-1}) was at least 10 times higher than previously reported using electrochemical and ECL methods with different amplification strategies.[45,46] As the normal level of CEA in human serum is approximately 5 ng mL^{-1},[42] it is useful in diagnostic evaluations to avoid the possibility of false positives caused by sample dilution when the CEA concentration is elevated due to the onset or recurrence of a tumor.

Reproducibility, Stability, and Specificity of the PEC Biosensor. The coefficients of variation were determined by measuring samples with the same concentrations using five electrodes prepared independently under identical experimental conditions. The coefficients of variation for intra-assay runs of 0.05 and 5.0 μg mL^{-1} CEA (n = 5) were 4.9% and 4.7%, respectively, whereas the interassay coefficients of variation were 7.4% and 8.1%, respectively. These results suggest that the PEC biosensor possessed precision and fabrication reproducibility. When the PEC biosensor was stored away from direct light at 4 °C for 2 weeks, 93.7% of its initial response was maintained, and 88.1% of its initial response was retained after 3 weeks, indicating satisfactory long-term stability.

In addition, the selectivity of the PEC biosensor was evaluated by the photocurrent ($\Delta I = I_{0.005} - I_0$, where $I_{0.005}$ is the photocurrent of C_{CEA} = 0.005 μg mL^{-1} and I_0 is the photocurrent of C_{CEA} = 0 μg mL^{-1}) at 0.005 μg mL^{-1} CEA (Figure 6). α-Fetoprotein (AFP), carbohydrate antigen 125

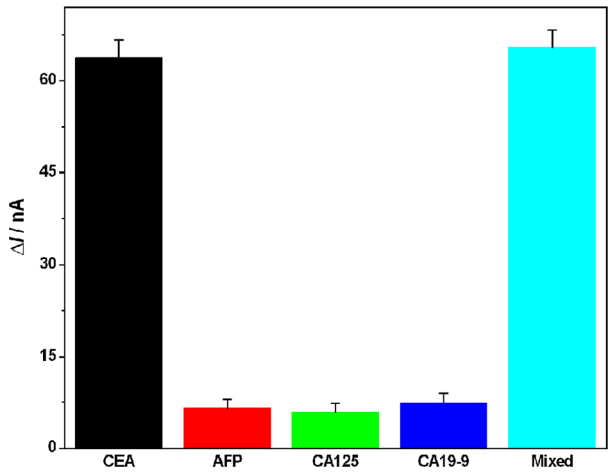

Figure 6. PEC response of the proposed biosensor to CEA with interfering agents, including AFP, CA125, and CA19-9 at the same concentration (0.005 μg mL^{-1}). The concentration of interfering agents (0.1 μg mL^{-1}) was 20 times the concentration of CEA (0.005 μg mL^{-1}) in the mixed sample. The error bars show the relative standard deviations of four replicate experiments.

(CA125), and carbohydrate antigen 19-9 (CA19-9) were acted as three types of interfering agents. At the same concentration (0.005 μg mL^{-1}), the PEC responses to AFP, CA125, and CA19-9 were only 10.3%, 9.3%, and 11.4%, respectively, compared to that to CEA, implying a negligible interference of these tumor markers. When the concentration of interfering agents (0.1 μg mL^{-1}) was greater than 20-fold higher than that of CEA (0.005 μg mL^{-1}) in the mixed sample, the photocurrent was 102.6% of the photocurrent in the presence of CEA (0.005

Table 1. Comparison of Serum CEA Levels Determined Using the Reference and Proposed Methods

	sample 1	sample 2	sample 3	sample 4	sample 5
reference method (ng mL^{-1})	3731	373.1	37.31	7. 462	3.731
proposed method[a] (ng mL^{-1})	4061 ± 31.3	339.2 ± 8.8	34.82 ± 2.87	8.259 ± 1.174	4.175 ± 0.927
relative error (%)	8.8	−9.1	6.7	10.7	11.9

[a]Average value from five successive determinations; serum samples 2, 3, 4, and 5 were diluted 10-, 100-, 500-, and 1000-fold, respectively.

μg mL^{-1}) alone. These results illustrate that only CEA, excluding other test samples, could cause obvious differences in the PEC response, verifying the good selectivity of the PEC biosensor toward CEA detection.

Analysis of Clinical Samples. This PEC biosensor was successfully used for clinical sample detection. When the level of CEA in serum was greater than the calibration range, the serum samples were appropriately diluted with Tris−HCl buffer saline (0.01 mol L^{-1}, pH 7.4) prior to the assay being performed. The assay results for clinical serum samples, compared with the reference values obtained using a commercial ECL immunoassay, showed an acceptable agreement with relative errors of less than 11.9% (Table 1), indicating the acceptable accuracy of the proposed PEC biosensor for clinical sample detection.

CONCLUSIONS

In summary, an innovative PEC biosensor platform was developed by the in situ generation of CdS QDs on GO using enzymatic reactions, which offered a "green" alternative to inconvenient presynthesis procedures for the fabrication of semiconducting nanoparticles. Combined with biological recognition, the strategy was successfully applied to CEA determination, which was based on the PEC activity of CdS QDs sensitized GO with satisfactory performance. This work provides a new opportunity for the development of numerous rapid and convenient analytical techniques using the PEC method based on the readout signal and may be applied as an excellent initial design for the preparation of various solar-energy-driven applications, including PEC water splitting, photocatalysis, and solar cell design.

AUTHOR INFORMATION

Corresponding Author

*Phone/fax: +86-25-85891051. E-mail: daizhihuii@njnu.edu.cn.

Notes

The authors declare no competing financial interest.

ACKNOWLEDGMENTS

This work was supported by the National Natural Science Foundation of China (Grants 21475062, 21175069, and 21205061), Natural Science Foundation of Jiangsu (Grant BK2012448), and Foundation of the Jiangsu Education Committee (Grant 11KJA150003). We appreciate the financial support from the Priority Academic Program Development of Jiangsu Higher Education Institutions.

REFERENCES

(1) Tan, S. C.; Crouch, L. I.; Jones, M. R.; Well, M. Generation of Alternating Current in Response to Discontinuous Illumination by Photoelectrochemical Cells Based on Photosynthetic Proteins. *Angew. Chem., Int. Ed.* **2012**, *51*, 6667−6671.

(2) Wang, F.; Liu, X. Q.; Willner, I. Integration of Photoswitchable Proteins, Photosynthetic Reaction Centers and Semiconductor/Biomolecule Hybrids with Electrode Supports for Optobioelectronic Applications. *Adv. Mater.* **2013**, *25*, 349−377.

(3) Long, Y.-T.; Kong, C.; Li, D.-W.; Li, Y.; Chowdhury, S.; Tian, H. Ultrasensitive Determination of Cysteine Based on the Photocurrent of Nafion-Functionalized CdS-MV Quantum Dots on an ITO Electrode. *Small* **2011**, *7*, 1624−1628.

(4) Gill, R.; Zayats, M.; Willner, I. Semiconductor Quantum Dots for Bioanalysis. *Angew. Chem., Int. Ed.* **2008**, *47*, 7602−7625.

(5) Li, Y.-J.; Ma, M.-J.; Zhu, J.-J. Dual-Signal Amplification Strategy for Ultrasensitive Photoelectrochemical Immunosensing of α-Fetoprotein. *Anal. Chem.* **2012**, *84*, 10492−10499.

(6) Tu, W. W.; Wang, W. J.; Lei, J. P.; Deng, S. Y.; Ju, H. X. Chemiluminescence Excited Photoelectrochemistry Using Graphene-Quantum Dots Nanocomposite for Biosensing. *Chem. Commun.* **2012**, *48*, 6535−6537.

(7) Zhao, X. M.; Zhou, S. W.; Jiang, L.-P.; Hou, W. H.; Shen, Q. M.; Zhu, J.-J. Graphene-CdS Nanocomposites: Facile One-Step Synthesis and Enhanced Photoelectrochemical Cytosensing. *Chem.—Eur. J.* **2012**, *18*, 4974−4981.

(8) Chen, D.; Zhang, H.; Li, X.; Li, J. H. Biofunctional Titania Nanotubes for Visible-Light-Activated Photoelectrochemical Biosensing. *Anal. Chem.* **2010**, *82*, 2253−2261.

(9) Kang, Q.; Yang, L. X.; Chen, Y. F.; Luo, S. L.; Wen, L. F.; Cai, Q. Y.; Yao, S. Z. Photoelectrochemical Detection of Pentachlorophenol with a Multiple Hybrid $CdSe_xTe_{1-x}/TiO_2$ Nanotube Structure-Based Label-Free Immunosensor. *Anal. Chem.* **2010**, *82*, 9749−9754.

(10) Liang, Y.; Kong, B.; Zhu, A. W.; Wang, Z.; Tian, Y. A Facile and Efficient Strategy for Photoelectrochemical Detection of Cadmium Ions Based on in Situ Electrodeposition of CdSe Clusters on TiO_2 Nanotubes. *Chem. Commun.* **2012**, *48*, 245−247.

(11) Tang, J.; Kong, B.; Wang, Y. C.; Xu, M.; Wang, Y. L.; Wu, H.; Zheng, G. F. Photoelectrochemical Detection of Glutathione by IrO_2−Hemin−TiO_2 Nanowire Arrays. *Nano Lett.* **2013**, *13*, 5350−5354.

(12) Zhao, W.-W.; Tian, C.-Y.; Xu, J.-J.; Chen, H.-Y. The Coupling of Localized Surface Plasmon Resonance-Based Photoelectrochemistry and Nanoparticle Size Effect: Towards Novel Plasmonic Photoelectrochemical Biosensing. *Chem. Commun.* **2012**, *48*, 895−897.

(13) Li, H. B.; Li, J.; Xu, Q.; Hu, X. Y. Poly(3-hexylthiophene)/TiO_2 Nanoparticle-Functionalized Electrodes for Visible Light and Low Potential Photoelectrochemical Sensing of Organophosphorus Pesticide Chlopyrifos. *Anal. Chem.* **2011**, *83*, 9681−9686.

(14) Zhao, W.-W.; Ma, Z.-Y.; Xu, J.-J.; Chen, H.-Y. In Situ Modification of a Semiconductor Surface by an Enzymatic Process: A General Strategy for Photoelectrochemical Bioanalysis. *Anal. Chem.* **2013**, *85*, 8503−8506.

(15) Zhang, X. R.; Xu, Y. P.; Yang, Y. Q.; Jin, X.; Ye, S. J.; Zhang, S. S.; Jiang, L. L. A New Signal-On Photoelectrochemical Biosensor Based on a Graphene/Quantum-Dot Nanocomposite Amplified by the Dual-Quenched Effect of Bipyridinium Relay and AuNPs. *Chem.—Eur. J.* **2012**, *18*, 16411−16418.

(16) Wu, Y. P.; Zhang, B. T.; Guo, L.-H. Label-Free and Selective Photoelectrochemical Detection of Chemical DNA Methylation Damage Using DNA Repair Enzymes. *Anal. Chem.* **2013**, *85*, 6908−6914.

(17) Ge, S. G.; Yu, J. H.; Yan, M.; Huang, J. D. A Paper-Based Photoelectrochemical Immunoassay for Low-Cost and Multiplexed Point-of-Care Testing. *Chem. Commun.* **2013**, *49*, 3294−3296.

(18) Li, Y.-J.; Ma, M.-J.; Yin, G.; Kong, Y.; Zhu, J.-J. Phthalocyanine-Sensitized Graphene-CdS Nanocomposites: An Enhanced Photo-

electrochemical Immunosensing Platform. *Chem.—Eur. J.* **2013**, *19*, 4496−4505.
(19) Zhao, W.-W.; Zhang, L.; Xu, J.-J.; Chen, H.-Y. Cell Surface Carbohydrates Evaluation via a Photoelectrochemical Approach. *Chem. Commun.* **2012**, *48*, 9456−9458.
(20) Yang, Y. J.; Xiang, J. W. Template-Free Synthesis of CuS Nanorods with a Simple Aqueous Reaction at Ambient Conditions. *Appl. Phys. A: Mater. Sci. Process.* **2005**, *81*, 1351−1353.
(21) Yang, Y. J. The Thioglycerol Catalyzed Reaction of Metal Salts and Elemental Sulfur: A New Approach for the Preparation of Nanocrystalline Metal Sulfides. *Colloids Surf., A* **2006**, *276*, 192−196.
(22) Saa, L.; Pavlov, V. Enzymatic Growth of Quantum Dots: Applications to Probe Glucose Oxidase and Horseradish Peroxidase and Sense Glucose. *Small* **2012**, *8*, 3449−3455.
(23) Saa, L.; Virel, A.; Sanchez-Lopez, J.; Pavlov, V. Analytical Applications of Enzymatic Growth of Quantum Dots. *Chem.—Eur. J.* **2010**, *16*, 6187−6192.
(24) Malashikhina, N.; Garai-Ibabe, G.; Pavlov, V. Unconventional Application of Conventional Enzymatic Substrate: First Fluorogenic Immunoassay Based on Enzymatic Formation of Quantum Dots. *Anal. Chem.* **2013**, *85*, 6866−6870.
(25) Karim, M. R.; Hatakeyama, K.; Matsui, T.; Takehira, H.; Taniguchi, T.; Koinuma, M.; Matsumoto, Y.; Akutagawa, T.; Nakamura, T.; Noro, S.; Yamada, T.; Kitagawa, H.; Hayami, S. Graphene Oxide Nanosheet with High Proton Conductivity. *J. Am. Chem. Soc.* **2013**, *135*, 8097−8100.
(26) Radich, J. G.; Kamat, P. V. Making Graphene Holey. Gold-Nanoparticle-Mediated Hydroxyl Radical Attack on Reduced Graphene Oxide. *ACS Nano* **2013**, *6*, 5546−5557.
(27) Bang, J.; Meng, S.; Sun, Y.-Y.; West, D.; Wang, Z. G.; Gao, F.; Zhang, S. B. Regulating Energy Transfer of Excited Carriers and the Case for Excitation-Induced Hydrogen Dissociation on Hydrogenated Graphene. *Proc. Natl. Acad. Sci. U.S.A.* **2013**, *110*, 908−911.
(28) Li, Q.; Guo, B. D.; Yu, J. G.; Ran, J. R.; Zhang, B. H.; Yan, H. J.; Gong, J. R. Highly Efficient Visible-Light-Driven Photocatalytic Hydrogen Production of CdS-Cluster-Decorated Graphene Nanosheets. *J. Am. Chem. Soc.* **2011**, *133*, 10878−10884.
(29) Lightcap, I. V.; Kamat, P. V. Fortification of CdSe Quantum Dots with Graphene Oxide. Excited State Interactions and Light Energy Conversion. *J. Am. Chem. Soc.* **2012**, *134*, 7109−7116.
(30) Chen, D.; Feng, H. B.; Li, J. H. Graphene Oxide: Preparation, Functionalization, and Electrochemical Applications. *Chem. Rev.* **2012**, *112*, 6027−6053.
(31) Ocsoy, I.; Gulbakan, B.; Chen, T.; Zhu, G. Z.; Chen, Z.; Sari, M. M.; Peng, L.; Xiong, X. L.; Fang, X. H.; Tan, W. H. DNA-Guided Metal-Nanoparticle Formation on Graphene Oxide Surface. *Adv. Mater.* **2013**, *25*, 2319−2325.
(32) Wang, Y.; Lu, J.; Tang, L. H.; Chang, H. X.; Li, J. H. Graphene Oxide Amplified Electrogenerated Chemiluminescence of Quantum Dots and Its Selective Sensing for Glutathione from Thiol-Containing Compounds. *Anal. Chem.* **2009**, *81*, 9710−9715.
(33) Lu, W.; Jin, Y.; Wang, G.; Chen, D.; Li, J. H. Enhanced Photoelectrochemical Method for Linear DNA Hybridization Detection Using Au-Nanopaticle Labeled DNA as Probe onto Titanium Dioxide Electrode. *Biosens. Bioelectron.* **2008**, *23*, 1534−1539.
(34) Wee, B.-H.; Hong, J.-D. A Method for Fabricating an Ultrathin Multilayer Film Composed of Poly(*p*-phenylenevinylene) and Reduced Graphene Oxide on a Plastic Substrate for Flexible Optoelectronic Applications. *Adv. Funct. Mater.* **2013**, *23*, 4657−4666.
(35) Malig, J.; Jux, N.; Kiessling, D.; Cid, J.-J.; Vázquez, P.; Torres, T.; Guldi, D. M. Towards Tunable Graphene/Phthalocyanine-PPV Hybrid Systems. *Angew. Chem., Int. Ed.* **2011**, *50*, 3561−3565.
(36) Kovtyukhova, N. I.; Ollivier, P. J.; Martin, B. R.; Mallouk, T. E.; Chizhik, S. A.; Buzaneva, E. V.; Gorchinskiy, A. D. Layer-by-Layer Assembly of Ultrathin Composite Films from Micron-Sized Graphite Oxide Sheets and Polycations. *Chem. Mater.* **1999**, *11*, 771−778.
(37) Tiwari, J. N.; Nath, K.; Kumar, S.; Tiwari, R. N.; Kemp, K. C.; Le, N. H.; Youn, D. H.; Lee, J. S.; Kim, K. S. Stable Platinum Nanoclusters on Genomic DNA-Graphene Oxide with a High Oxygen Reduction Reaction Activity. *Nat. Commun.* **2013**, *4*, 2221.
(38) Wang, H. L.; Robinson, J. T.; Li, X. L.; Dai, H. J. Solvothermal Reduction of Chemically Exfoliated Graphene Sheets. *J. Am. Chem. Soc.* **2009**, *131*, 9910−9911.
(39) Yang, Z. J.; Liu, H.; Zong, C.; Yan, F.; Ju, H. X. Automated Support-Resolution Strategy for a One-Way Chemiluminescent Multiplex Immunoassay. *Anal. Chem.* **2009**, *81*, 5484−5489.
(40) Wang, F.; Wang, W.-G.; Wang, X.-J.; Wang, H.-Y.; Tung, C.-H.; Wu, L.-Z. A Highly Efficient Photocatalytic System for Hydrogen Production by a Robust Hydrogenase Mimic in an Aqueous Solution. *Angew. Chem., Int. Ed.* **2011**, *123*, 3193−3197.
(41) Ambrosi, A.; Pumera, M. Precise Tuning of Surface Composition and Electron-Transfer Properties of Graphene Oxide Films through Electroreduction. *Chem.—Eur. J.* **2013**, *19*, 4748−4753.
(42) Hu, W. H.; Liu, Y. S.; Lu, Z. S.; Li, C. M. Poly[oligo(ethylene glycol) methacrylate-*co*-glycidyl methacrylate] Brush Substrate for Sensitive Surface Plasmon Resonance Imaging Protein Arrays. *Adv. Funct. Mater.* **2010**, *20*, 3497−3503.
(43) Ho, J. A. A.; Lin, Y. C.; Wang, L. S.; Hwang, K. C.; Chou, P. T. Carbon Nanoparticle Enhanced Immunoelectrochemical Detection for Protein Tumor Marker with Cadmium Sulfide Biotracers. *Anal. Chem.* **2009**, *81*, 1340−1346.
(44) Yan, M.; Ge, L.; Gao, W. Q.; Yu, J. H.; Song, X. R.; Ge, S. G.; Jia, Z. Y.; Chu, C. C. Electrogenerated Chemiluminescence from a Phenyleneethynylene Derivative and Its Ultrasensitive Immunosensing Application Using a Nanotubular Mesoporous Pt-Ag Alloy for Signal Amplification. *Adv. Funct. Mater.* **2012**, *22*, 3899−3906.
(45) Deng, S. Y.; Hou, Z. T.; Lei, J. P.; Lin, D. J.; Hu, Z.; Yan, F.; Ju, H. X. Signal Amplification by Adsorption-Induced Catalytic Reduction of Dissolved Oxygen on Nitrogen-Doped Carbon Nanotubes for Electrochemiluminescent Immunoassay. *Chem. Commun.* **2011**, *47*, 12107−12109.
(46) Chikkaveeraiah, B. V.; Bhirde, A. A.; Morgan, N. Y.; Eden, H. S.; Chen, X. Y. Electrochemical Immunosensors for Detection of Cancer Protein Biomarkers. *ACS Nano* **2012**, *6*, 6546−6561.